Molecular Dynamics Simulations of Crumpling Polymer Grafted Graphene Sheets: Implications for Functional Nanocomposites

Yangchao Liao [1, 2], Oriana Molares Palmero [3], Amara Arshad [4], Long Chen [5], Wenjie Xia [5, *]

[1] Department of Civil, Construction and Environmental Engineering, North Dakota State University, Fargo, ND 58108, United States

[2] Applied Mechanics Laboratory, Department of Engineering Mechanics, Tsinghua University, Beijing 100084, China

[3] J. Crayton Pruitt Family Department of Biomedical Engineering, University of Florida, Gainesville, FL 32611, United States

[4] Materials and Nanotechnology, North Dakota State University, Fargo, ND 58108, United States

[5] Department of Aerospace Engineering, Iowa State University, Ames, IA 50011, United States

* Corresponding author. E-mail: wxia@iastate.edu

Abstract

Polymer-grafted graphene (PgG) sheets are of interest in the development of functional nanocomposite materials for sensing, energy storage, and coatings. Although extensive studies have reported on the electrical, thermal, and mechanical behaviors of PgG sheets, our understanding of the fundamental structural behavior of crumpled PgG sheets is still lacking. Here we perform molecular dynamics (MD) simulations of the crumpling behavior of poly(methyl methacrylate) (PMMA) grafted graphene (PMMA-g-G) sheets with varying grafting densities based on previously developed coarse-grained (CG) models of PMMA and graphene. The simulation results reveal that the conformation of PMMA-g-G sheets in the initial equilibrium is controlled by the PMMA grafting density and can be divided into three different regimes (i.e., flat, folded, and wrinkled states), and that the local distribution of PMMA on the graphene affects the local curvature of the sheet. By analyzing the total potential energy, shape descriptor, and conformation of the system during the crumpling process, it is found that the increase in grafting density reduces the self-adhering and self-folding behaviors of the sheet, while making the bending behavior dominate the crumpling process. Moreover, the evaluation of the local curvature and stress distributions, and cross-sectional patterns of crumpled PMMA-g-G sheets further uncovers the reduced degree of mechanical heterogeneity due to the increased grafting density. Our study provides fundamental insights into the conformational behavior of PMMA-g-G sheets in equilibrium and crumpled states in relation to grafting density, which is crucial for establishing the structure-property relationships for leveraging crumpled polymer-grafted sheets in functional nanocomposites.

Keywords Coarse-grained modeling; Molecular dynamics simulations; Polymer grafted graphene sheet; Crumpling behavior; Mechanical state

1. Introduction

Graphene, a two-dimensional (2D) honeycomb crystal structure, is composed of four carbon atoms in sp^2 hybridization connected by covalent bonds.[1] Graphene has exceptional mechanical,[2] electrical,[3] thermal,[4] and optoelectronic properties[5] due to its structural characteristics. This, coupled with its high theoretical specific surface area,[6] accredits graphene's wide application in functional nanocomposites,[7] impact protection,[8] biomedicine,[9] energy storage,[10] electronics,[11] and other engineering applications. In addition, graphene is often incorporated into polymer matrices to construct high-performance polymer nanocomposites due to superior chemical and interfacial interactions, which enables more efficient use of graphene's properties.[12] In most previous studies, graphene/polymer nanocomposites were prepared by a solution method,[13] melting method,[14] *in-situ* polymerization method,[15] and electrochemical reaction method,[16] each of which require adequate mixing of graphene and polymer.[17] However, the strong π-π conjugations between graphene sheets and the huge aspect ratio of graphene complicate the material's dispersion in organic matrices, especially for macro graphene.[18] The inhomogeneous distribution of graphene sheets in the matrix affects the performance of the nanocomposites.[17] In this regard, the volume-exclusion effect of the grafted molecules of polymer-grafted graphene (PgG) helps to reduce such interlayer interaction and facilitate the dispersion of graphene in the solvent and the polymer.[19] The properties of PgG sheets are influenced by various factors such as polymer type, grafting method, and polymer distribution state.[20] Moreover, graphene sheets tend to develop different degrees of corrugations and crumples in the presence of solvents,[21] substrates,[22] edge stresses,[23] and defects,[24] and these corrugated conformations also control the performance of PgG sheets.[25,26]

Most recent efforts have focused on exploring the grafting approach and grafting ability of PgG sheets, as well as their thermal, electrical, and mechanical properties.[7,13,27] Currently, there are two mainstream approaches for the preparation of covalent PgG, namely the "grafting to" approach[28] and the "grafting from" approach.[29] Specifically, the "grafting to" approach relates to radical coupling or reaction with edge-bound carboxylic acid groups on a nanosheet, and the "grafting from" approach involves initiator-functionalized graphene for polymerization. The "grafting to" approach is reported to produce well-defined and controllable grafted polymer chains with good processability and high grafting density, while the "grafting from" approach ensures the chain length and grafting density of the grafted polymer, which significantly improves the solvation strength of the polymer.[30] Moreover, Zhang *et al*. prepared conductive poly(methyl methacrylate) (PMMA) grafted reduced graphene oxide (PMMA-g-RGO) nanosheets with grafting ratio up to 33.2%.[31] It was revealed that the surface grafting of PMMA-g-RGO suppressed the aggregation behavior of the nanosheets in the matrix and formed a conductive network in the poly (styrene-co-acrylonitrile) rich phase, optimizing the conductive properties of the system.[31] The polystyrene (PS) grafted graphene oxide (PS-g-GO) with high grafting density has a more uniform PS chain distribution compared to the system with low grafting density, and the 2 wt% graphene content corresponds to a significantly higher thermal conductivity of the PS-g-GO.[29] Remarkably, the PgG nanosheets enhanced the tensile strength and Young's modulus of the nanocomposites.[32] This is attributed to the chemical interfacial bonding between the PgG nanosheets and the matrix, which has led to the effective load transfer from the matrix to the nanosheets, allowing a low concentration of nanosheets to significantly strengthen the mechanical properties of the nanocomposites.[32,33] Furthermore, the PgG nanosheets added to the nanocomposites (e.g., poly(L-lactic acid))

have properties such as homogeneous dispersion, high interfacial area, and strong adhesion (caused by surface specific functional groups), and the obtained nanocomposites exhibit promoted cold crystallization behavior and improved glass transition temperature, melting temperature, flexural and tensile strengths.[34]

In addition to experimental studies, the molecular dynamics (MD) simulations are an effective approach to gain insight into the conformational, mechanical, thermal, and dynamical properties of complex nanocomposites.[35] These hold a critical role in understanding the relationship between morphology at the molecular level and morphology at the macroscopic scale.[36] In Liu *et al*., MD simulations demonstrated that PgG nanosheets with longer polymer chains formed an improved brick-mud structure to shield the inter-sheet van der Waals interactions, resulting in a more homogeneous dispersion in the polymer nanocomposites compared to the system with shorter polymer chains.[37] The increase in the chain length and the interaction strength between end functional groups of the grafted chains enhances the mechanical properties (*e.g.*, stress-strain behavior) and self-healing behaviors of the nanocomposites.[37] In general, graphene sheets functionalized with chemical groups improve mechanical and other functional properties due to the formation of covalent bonds with the polymer matrices,[38,39] while deteriorating the intrinsic thermal conductivity of graphene.[40] Furthermore, in Gao *et al*., MD simulations identified two sheet size-dependent regimes affecting the intrinsic thermal conductivity of nanocomposites: the "interface-dominated" regime for small sheet sizes and the "filler-dominated" regime for large sheet sizes.[41] To summarize, the functionalized sheet has an enhanced effect on the thermal conductivity of the system in the "interface-dominated" regime, while it is redundant in the "filler-dominated" regime.

Currently, several studies have highlighted the effects of polymer grafted nanosheets on the mechanical, electrical, and thermal properties of nanocomposites.[32,37,42] However, there is a lack of understanding on the conformational and crumpling behavior of polymer-grafted nanosheets. One would expect flat rather than crumpled polymer-grafted nanosheets to achieve greater surface properties. Nevertheless, this assumption is challenged since crumpled nanosheets have demonstrated enhanced compressive strength, [43,44,45] high electrical and thermal conductivity,[46,47,48] and considerable light absorption[49] compared to flat nanosheets. Crumpled sheets are desirable nanostructures for chemical activity enhancement,[26] friction modification,[50] and energy storage.[51] Hence, the study of crumping behavior has practical significance for polymer grafted nanosheets research.

In this study, we adopt the coarse-grained (CG) MD modeling technique to investigate the crumpling behaviors of PMMA grafted graphene (PMMA-g-G) sheets with various grafting densities. Specifically, we employ the CG models of PMMA chains[52] and graphene sheets,[53] which were previously developed on the fundamental atomic models of PMMA and graphene, respectively. With these models, we develop a CG PMMA-g-G sheet model by bonding one end of a CG PMMA chain to a CG graphene sheet. In our MD simulations, the crumpling process is implemented by reducing the volume of the confining sphere comprising the CG PMMA-g-G model, which mimics the aerosol evaporation method commonly used in experiments to prepare crumpled nanosheets.[54] By evaluating the conformational and shape properties of PMMA-g-G sheets with different grafting densities in the initial equilibrium, we obtain three grafting density-dependent regimes describing the conformation of PMMA-g-G sheets: flat, folded, or wrinkled states. To understand the mechanisms that develop the different conformational regimes, we analyse the relationship between the local distribution of PMMA and the local curvature of

graphene sheets of the equilibrated system. Through evaluation of the total potential energy and shape descriptor of PMMA-g-G sheets during crumpling, we can deconvolute the grafting density-influenced crumpling behaviors, *i.e.*, self-adhering-dominated and bending-dominated crumpling processes. We further discuss the local curvature, local stresses, and cross-section patterns the crumpled PMMA-g-G spheres to reveal the stress heterogeneity governed by the grafting density. Our study highlights the critical effect of grafting density on the initial conformation and crumpling behavior of PMMA-g-G sheets, which will aid in the tailored design of crumpled polymer grafted nanosheets for functional nanocomposite applications.

2. Computational Methods

2.1. Overview of coarse-grained modeling

To overcome the spatial and temporal constraints while preserving the fundamental molecular features, we employ our previously developed PMMA and graphene CG models to build the CG model of PMMA-g-G sheet.[52,53] Specifically, as shown in **Figure 1(a)**, the CG model of PMMA has a two-bead per monomer mapping scheme, *i.e.*, one bead represents the backbone group and the other bead represents the sidechain methyl group. The bonded interactions (*i.e.*, bond, angle, and dihedral potentials) of the PMMA CG model are parameterized by the inverse Boltzmann method in order to match the probability distributions from atomistic trajectories; the non-bonded interaction of the model has the form of a 12-6 Lennard-Jones (LJ) potential, which is parameterized to capture the essential thermo-mechanical properties.[52] Moreover, the CG model of graphene is derived based on a 4-to-1 mapping scheme, where every four carbon atoms are represented by one CG bead (see **Figure 1(a)**). As the hexagonal symmetry of the atomic lattice is conserved, the graphene CG model can effectively capture the elasticity, interlayer shear,

adhesion, and fracture properties of graphene sheets.[26,53,55,56] Notably, the CG models for PMMA and graphene adopted in this paper are 2-3 orders of magnitude more computationally efficient than the corresponding atomistic models. Information regarding the force fields of the CG PMMA and CG graphene models are detailed in the previous studies.[52,53]

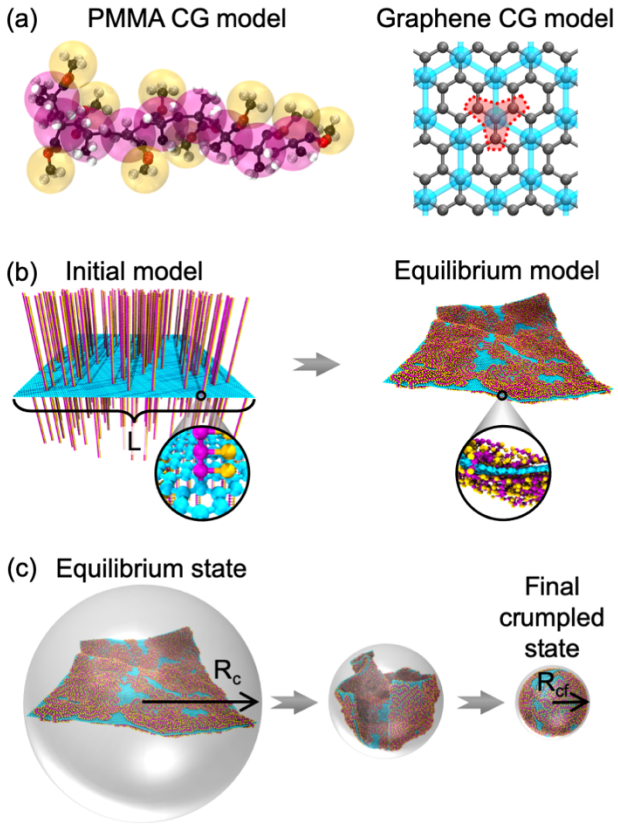

Figure 1. Schematics of CG-MD modeling. **(a)** All-atomistic (AA) to CG mapping schemes for PMMA chain (left) and graphene sheet (right). **(b)** Initially constructed (left) and fully equilibrated (right) CG PMMA-g-G sheet model, where PMMA chains (70 monomers per chain) are randomly grafted on both sides of the graphene sheet (edge length $L = 50.2$ nm). The zoom-in show one end of the CG PMMA chain bonded to the CG graphene sheet, and the CG PMMA chains adsorbed on both sides of the CG graphene sheet, respectively. **(c)** Conformational evolution of the crumpling process of equilibrated PMMA-g-G sheet model, where the translucent gray spheres represent virtual boundaries that exert repulsive forces on the model, and which confine the model to three-dimensional spaces. R_c and R_{cf} represent the radius of the confining sphere during the crumpling process and at the final crumpled state, respectively.

The initially constructed PMMA-g-G sheet model consists of a square CG graphene sheet and straight CG PMMA chains. As illustrated in **Figure 1(b)**, the straight PMMA chains with 70 monomers per chain are randomly bonded on both sides of the square graphene sheet having an edge length of 50.2 nm (*i.e.*, $L = 50.2$ nm). The bond potential of the bonds connecting the PMMA chains to the graphene is consistent with the bond potential of the graphene model. Moreover, the non-bonded interaction between PMMA and graphene is represented by the 12-6 LJ potential, $V_{nb}(r)$, observed in previous studies:[26,56]

$$V_{nb}(r) = 4\varepsilon\left[\left(\frac{\sigma}{r}\right)^{12} - \left(\frac{\sigma}{r}\right)^{6}\right], \text{ for } r < r_{cut} \quad (1)$$

where r is the distance between a PMMA bead and a graphene bead, and the cutoff distance r_{cut} is equal to 15 Å; ε is the potential well depth of the interaction between PMMA beads and graphene beads; σ is the distance at which $V_{nb}(r)$ crosses zero. In our simulations, $\varepsilon = 1.2$ kcal/mol and $\sigma = 4.5$ Å, which lead to an interfacial energy of approximately 0.2 J/m^2, comparable to the experimentally reported value between the PMMA matrix and the graphene sheets.[57] In the detailed molecular model, functionalization of graphene with reactive groups leads to covalent bonding with PMMA, resulting in composites with enhanced mechanical, thermal and electrical properties. Nonetheless, we focus on the non-bonded interaction rather than the bond interaction between PMMA and graphene, as the effect of the bond interaction on the sheet crumpling process can be neglected.[58]

The fidelity of our CG models for graphene and PMMA is ensured through a rigorous model development process based on AA counterparts, leading to a reasonably good approximation of both mechanical and thermodynamic characteristics pertinent to

each material.[52,53] Specifically, the CG model of graphene maintains the intrinsic hexagonal symmetry and anisotropic mechanical responses, while the PMMA CG model has been fine-tuned to yield the dynamics and glass-transition temperature, in good agreement with empirical observations and AA simulation data. Collectively, these thoroughly validated models substantiate the robustness and precision of our integrated PMMA-grafted graphene CG model.

2.2. Coarse-grained molecular dynamics simulation details

In the CG-MD simulations, the initially constructed PMMA-g-G sheet model is aligned with the *xy* plane (*z*-direction perpendicular to the graphene sheet) and located at the center of the simulation box with dimensions of 500 nm × 500 nm × 500 nm. The periodic boundary conditions apply to all directions. The time step and temperature of the simulation are 6 fs and 300 K, respectively. To relax the system, we first minimize the energy of the system using an iterative conjugate gradient algorithm, and then perform an equilibrium simulation in the NVT ensemble of 12 ns to ensure that the total potential energy of the system converges to an approximately invariant value. **Figure 1(b)** shows the conformations of the initially constructed and fully equilibrated and relaxed PMMA-g-G sheet model. After equilibration, the crumpling simulation is performed to study the crumpling behaviors of PMMA-g-G sheet.

Specifically, we apply a virtual confining sphere with variable volume to mimic the crumpling process for preparing crumpled nanosheets based on the aerosol evaporation approach.[54] As shown in **Figure 1(c)**, a confining sphere of radius R_c encompasses the PMMA-g-G sheet model, where its boundary exerts a repulsive force on the model at a certain cut-off distance. The sheet model is progressively compacted into a tight spherical

crumpled structure as the radius of the confining sphere decreases. In particular, the repulsive force $F(r_i)$ generated by the confining sphere can be described as follows:

$$F(r_i) = \begin{cases} -K_c(r_i - R_c)^2, \text{ for } r_i \geq R_c \\ 0, \text{ for } r_i < R_c \end{cases} \quad (2)$$

where r_i is the distance between the ith bead of the model and the center of the confining sphere, and $K_c = 2.31\times10^5$ kcal/(mol nm^3) is the spring force constant. In the crumpling simulation, R_c is set to decrease steadily at a rate of 50 m/s until R_c equals R_{cf}, at which the sheet reaches the final crumpled state. Here, R_{cf}, controlling the final crumpled state of the sheet, can be written as:

$$R_{cf} = \left[\frac{3}{4\pi}\left(\frac{M_{pmma}}{\rho_{pmma}} + \frac{M_{graphene}}{\rho_{graphene}}\right)\right]^{1/3} \quad (3)$$

where M_{pmma} and $M_{graphene}$ are the total masses of PMMA chains and graphene sheet, respectively; $\rho_{pmma} = 1.147$ g/cm^3 and $\rho_{graphene} = 2.267$ g/cm^3 are the bulk densities of equilibrium CG PMMA and graphite, respectively.[52,59] It can be seen that an increase in the grafting density of the PMMA (which makes M_{pmma} increase) leads to an increased R_{cf}.

Notably, tests on different decreasing rates of R_c show that a crumpling velocity of 50 m/s improves the computational speed of the simulation and simultaneously capture the basic crumpling behavior of the sheet at low velocities. More details about the crumpling simulation of nanosheets can be found in our previous studies.[58,59,60,61] All of the CG-MD simulations in this paper are carried out using the open-source package Large-scale Atomic/Molecular Massively Parallel Simulator (LAMMPS),[62] and the visualization of the CG-MD simulations is realized through Visual Molecular Dynamics (VMD).[63]

2.3. Property calculations

In this study, we reveal the effect of grafting density (g) on the crumpling behavior of PMMA-g-G sheets. Variable g is defined as the total number of PMMA chains grafted onto the unit area of the graphene sheet, which is measured in chains/nm^2.

Initially, we calculate the shape descriptor named relative shape anisotropy (κ^2) and the localized distribution of PMMA, denoted as d_p, for PMMA-g-G sheets in equilibrium. Specifically, the relative shape anisotropy κ^2 is computed as:

$$\kappa^2 = 1 - 3\frac{\Lambda_1\Lambda_2 + \Lambda_2\Lambda_3 + \Lambda_3\Lambda_1}{(\Lambda_1 + \Lambda_2 + \Lambda_3)^2} \tag{4}$$

where Λ_1, Λ_2, and Λ_3 are the principal eigenvalues of the gyration tensor and ranked in ascending order (*i.e.*, $\Lambda_1 \leq \Lambda_2 \leq \Lambda_3$). κ^2 has values between 0 and 1, and it depicts spherical ($\kappa^2 = 0$), planar symmetric ($\kappa^2 = 0.25$), and ideal rod ($\kappa^2 = 1$) conformations.[58,64] The shape descriptor characterizes the geometrical configuration of the material. Our discussion of the shape descriptor of PMMA-g-G helps to modulate the morphological characteristics of the material, which is essential for the design of high-performance sheets with specific mechanical, electronic, and thermal properties.

To understand the definition of d_p, we take the i^{th} bead of graphene as an example and calculate its local PMMA distribution ($d_{p,i}$). In summary, for every PMMA bead there is a corresponding bead i in the graphene sheet that are paired to ensure the shortest distance between the two. The distribution of PMMA at the i^{th} bead of graphene can be written as:

$$d_{p,i} = \frac{n_i}{N_{pmma}} \tag{5}$$

where the n_i is the number of PMMA beads that satisfy the above matching condition with graphene bead i; N_{pmma} is the total number of the PMMA beads. Note that d_p quantitatively describes the degree of aggregation of PMMA on the graphene sheet.

Then, we introduce the compaction ratio (ρ_g) to identify the compaction degree of the sheet upon crumpling, which can be defined as:

$$\rho_g = \frac{R_g - R_{gf}}{R_{g0} - R_{gf}} \tag{6}$$

where $R_g = \sqrt{\Lambda_1 + \Lambda_2 + \Lambda_3}$ is the radius of gyration of the sheet during the crumpling process; R_{g0} and R_{gf} are the radii of gyration of the sheet at the initial equilibrium and at the final crumpling state, respectively. The value of ρ_g ranges from 0 to 1, and a smaller value indicates a greater degree of compaction of the sheet.

In addition, the total potential energy increment per unit area (ΔPE) of the sheet can be calculated as:[60]

$$\Delta PE = \frac{PE - PE_0}{A_{graphene}} \tag{7}$$

where PE and PE_0 are, respectively, the total potential energy of the system during the crumpling process and at the initial equilibrium; $A_{graphene}$ is the surface area of the flat graphene sheet.

Finally, the von Mises stress σ_v can obtained as follows:[43,44,60]

$$\sigma_v = \sqrt{\frac{(\sigma_{11} - \sigma_{22})^2 + (\sigma_{22} - \sigma_{33})^2 + (\sigma_{33} - \sigma_{11})^2 + 6(\sigma_{12}{}^2 + \sigma_{23}{}^2 + \sigma_{31}{}^2)}{2}} \tag{8}$$

where σ_{ij} $(i, j = 1, 2, 3)$ is the components of stress tensor. Note that the von Mises stress is typically employed as a yielding criterion rather than a real stress and is normalized with respect to the volume of the system in this study. Unless stated otherwise, six independent

simulations are carried out to obtain the average of the target properties of PMMA-g-G sheets with different grafting densities.

3. Results and Discussion

3.1. Sheet conformation in equilibrium

We first study the effect of grafting density on the conformation of PMMA-g-G sheet at the initial equilibrium state. **Figure 2(a)** shows the representative conformations of PMMA-g-G sheets with grafting densities g of 0.004, 0.075, 0.15, 0.2, 0.3, and 0.4 chains/nm^2, respectively, in equilibrium. It can be observed that the sheet exhibits a relatively flat conformation for small grafting density (*e.g.*, $g = 0.004$ chains/nm^2), similar to pristine graphene sheets.[60,65] As g increases (0.75 to 0.2 chains/nm^2 as seen in **Figure 2(a)**) the sheets tend to exhibit a folded morphology. For larger g (*e.g.*, 0.3 and 0.4 chains/nm^2), the sheets develop more wrinkles and corrugations rather than more folding. In addition, **Figure 2(b)** presents the evolution of the shape descriptor of the sheets—the relative shape anisotropy κ^2—with the grafting density. It is observed that the conformation of the equilibrated PMMA-g-G sheets can be divided into three different regimes based on κ^2. Specifically, regime I ($0 \leq g \lesssim 0.05$ chains/nm^2) corresponds to a comparatively flat conformation as $\kappa^2 \approx 0.25$, where the morphology of the sheet is not impacted by the PMMA chains, and the sheet maintains large planar configuration. Regime II describes the folded conformation with a grafting density of 0.05 chains/nm^2 $\lesssim g \lesssim$ 0.275 chains/nm^2, where κ^2 is noticeably higher than 0.25. In regime II, the grafted PMMA chains are randomly adsorbed to the surface of the sheet during the equilibrium simulation, making the local bending stiffness of the sheet inhomogeneous,[34,66] and the sheet thus bends up and self-folds in the region of low bending stiffness. When the grafting density is greater than ~0.275 chains/nm^2 (regime III), the

sheet only develops significant wrinkles and corrugations, and κ^2 drops to approximately 0.25. For such systems with large grafting densities, the PMMA chains entangle and accumulate on the sheet after equilibration,[67] and this uneven aggregation of PMMA directs the sheet to wrinkle and deform.

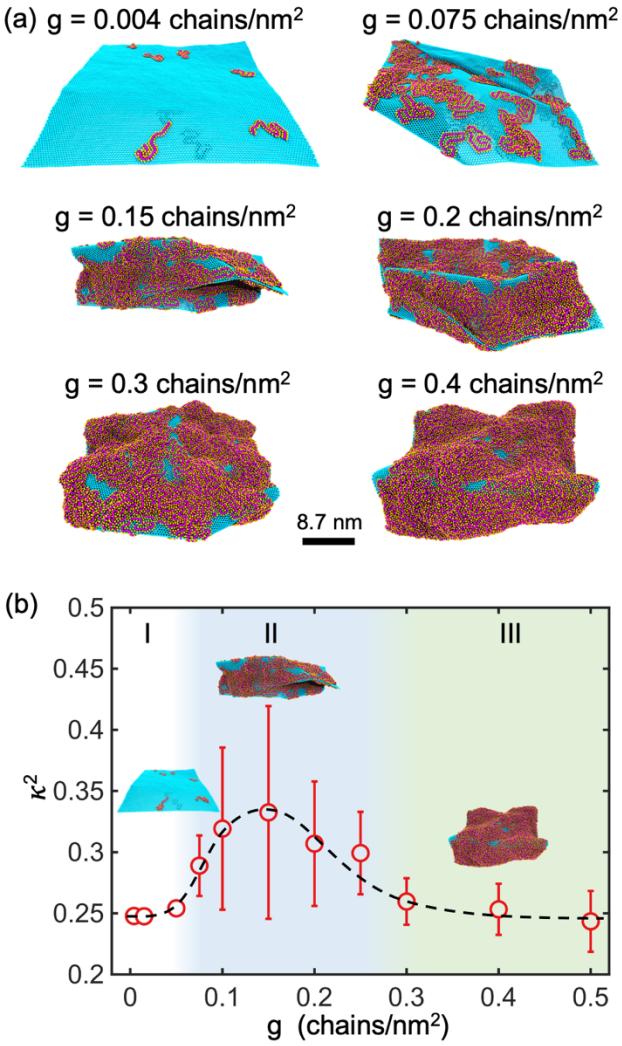

Figure 2. Effect of grafting density g on the conformation of the sheet in equilibrium. **(a)** Representative conformations of PMMA-g-G sheets (L = 50.2 nm) with g ranging from 0.004 to 0.4 chains/nm^2 in the equilibrium state. The black line represents the scale bar. **(b)** Variation of relative shape anisotropy κ^2 with respect to g of the sheets in the equilibrium state. Inset shows three typical conformations of sheets in regimes I, II, and III, respectively. The dashed curve shall guide the eye.

To better understand the above analyses, we further discuss the local distribution of PMMA d_p and the local curvature K for typical PMMA-g-G sheets in the three regimes. The d_p and K are mapped to a 2D planar model for better visualization. As shown in **Figure 3(a)** and **(b)**, the d_p and K of the sheet ($g = 0.004$ chains/nm^2) within regime I are uncorrelated. Interestingly, the d_p and K of the sheets in regimes II ($g = 0.15$ chains/nm^2) and III ($g = 0.4$ chains/nm^2) are highly correlated; in other words, the small d_p region corresponds to the large K region. Moreover, the sheet in regime II tends to develop regions of small d_p and large K in the zigzag direction (*i.e.*, horizontal direction), suggesting that the sheets are prone to folding along the zigzag direction [58]. Moreover, **Figure 3(c)** verifies the relationship between d_p and K for a sheet with $g = 0.4$ chains/nm^2, that is, a small PMMA distribution corresponds to a large curvature of the sheet.

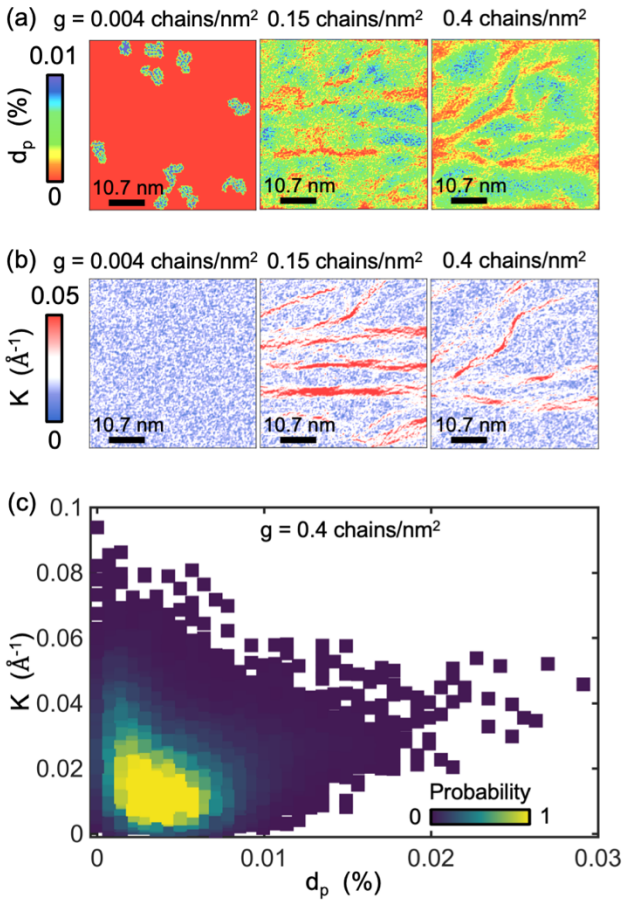

Figure 3. Grafting density g influenced PMMA distribution and sheet curvature. Maps of the **(a)** local distribution of PMMA d_p and **(b)** local curvature K for PMMA-g-G sheets ($L = 50.2$ nm) with different g in equilibrium. The corresponding conformation of the sheets is shown in Figure 2(a). The black lines denote the scale bar. **(c)** Distribution of d_p versus K for equilibrated PMMA-g-G sheet with $g = 0.4$ chains/nm^2. The probability values on the color scale are normalized by 5,000 to lie in the range of 0 to 1.

In general, the conformation of PMMA-g-G sheets with small grafting density (regime I) is not affected by PMMA chains. However, the PMMA chains randomly adsorbed and aggregated on the sheet control the folding and wrinkling of the system when the grafting density reaches a certain range (regimes II and III). This can be explained as the inhomogeneous polymer distribution and accumulation enable the sheet to fold and wrinkle by affecting the local bending stiffness of the sheet.[34,66] Furthermore, it is important

to note that the polymer's chain length may influence the sheet's curvature variations by impacting the local polymer distribution across the sheet.

3.2. Evaluation of crumpling process

We analyse the total potential energy and shape descriptor of PMMA-g-G sheets during the crumpling process to understand the grafting density-dependent crumpling behavior of the sheet. **Figure 4(a)** presents the variation of total potential energy increment per unit area ΔPE of PMMA-g-G sheets with different grafting densities g during the crumpling process. It can be found that the change of ΔPE at the early stage of the crumpling ($0.7 \lesssim \rho_g \leq 1$) is negligible; the ΔPE of the sheet with $g = 0.004$ chains/nm^2 shows a pronounced decrease at the intermediate stage of the crumpling ($0.2 \lesssim \rho_g \lesssim 0.7$), while the ΔPE tends to increase for the sheets with larger g (0.15 chains/nm^2 and 0.4 chains/nm^2); the ΔPE increases sharply at the late stage of the crumpling process due to further compression. This can be interpreted as the adhesion energy of the sheet with low grafting density (in regime I) dominates the intermediate crumpling process, resulting in a distinct valley in ΔPE.[58,68,69] In contrast, the entire crumpling process of the sheet with higher grafting density (in regimes II and III) is dominated by the bending energy, making ΔPE show an increasing trend in both the intermediate and late stages of crumpling.

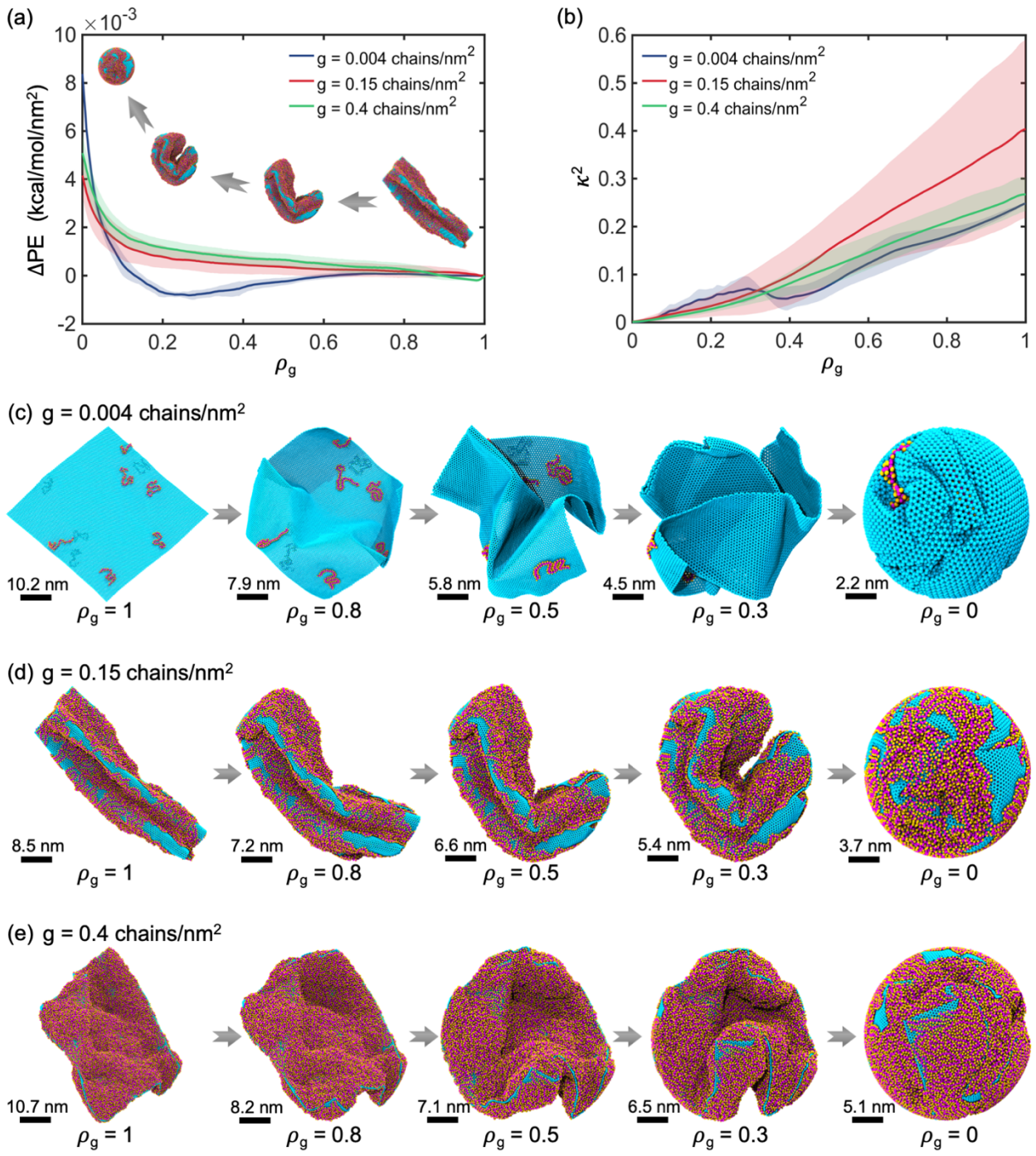

Figure 4. Evolution of the total potential energy and conformation of the system during crumpling. **(a)** Variation of total potential energy increment per unit area ΔPE with the compaction ratio ρ_g for the PMMA-g-G sheets having various grafting densities g. The inset shows a schematic of the crumpling process of a sheet with $g = 0.15$ chains/nm^2. **(b)** The relative shape anisotropy κ^2 as a function of ρ_g for PMMA-g-G sheets having different g. Shaded areas correspond to the standard deviation of PMMA-g-G sheets from six

independent crumpling simulations for each specific g. Representative conformations of crumpled PMMA-g-G sheets for different ρ_g (1, 0.8, 0.5, 0.3, and 0) with **(c)** $g = 0.004$ chains/nm^2, **(d)** $g = 0.15$ chains/nm^2, and **(e)** $g = 0.4$ chains/nm^2. The gray arrow denotes the direction in which the crumpling proceeds, and the black line represents the scale bar.

To better characterize the effect of grafting density on the structural features of PMMA-g-G sheets, the relative shape anisotropy κ^2 and representative conformation are evaluated for the sheets during crumpling. Generally, as shown in **Figure 4(b)**, the κ^2 of PMMA-g-G sheet shows a decreasing tendency to zero throughout the crumpling process, as equilibrated sheet is compacted into a crumpled sphere. In particular, the κ^2 of the sheet having smaller g (0.004 chains/nm^2) rebounded and formed a peak at the intermediate stage of the crumpling, which is attributed to the self-adhering and self-folding behaviors of the sheet; the κ^2 of the sheet with larger g (0.15 and 0.4 chains/nm^2) smoothly decreased to zero, implying the reduced self-adhering and self-folding behaviors and increased bending behavior. **Figure 4(c)-(e)** show representative conformations of the sheets with grafting densities of 0.004, 0.15, and 0.4 chains/nm^2 during the crumpling process, respectively. It is observed that the sheet with small grafting density (0.004 chains/nm^2) has similar crumpling conformations as the pristine graphene,[59,60] *e.g.*, the four corners of the sheet bend up significantly at the beginning of the crumpling (*e.g.*, $\rho_g = 0.8$ in **Figure 4(c)**), and the sheet forms large planar regions due to self-adhesion in the intermediate stage of the crumpling (*e.g.*, $\rho_g = 0.3$ in **Figure 4(c)**). In contrast, the sheet exhibits a bending-dominated crumpling mode during the entire compaction process for large grafting densities (0.15 and 0.4 chains/nm^2), *e.g.*, the ends of the rod-like model in **Figure 4(d)** bent

up and squeezed toward the middle, and the edges of the sheet in **Figure 4(e)** bent up and squeezed into a spherical shape.

In general, the grafting density of PMMA-g-G sheets influences the self-adhering and self-folding behaviors of the system during the crumpling process. Briefly, the sheet in regime I (see **Figure 2(b)**) possesses significant self-adhering and self-folding behaviors, and the adhesion of the system dominates the crumpling. On the contrary, self-adhering and self-folding behaviors of the sheets in regimes II and III are minimized and replaced by the bending behavior.

3.3. Grafting density affected mechanical state

We proceed to analyze the local curvature K, the local Von Mises stress σ_v, and the cross-section patterns of the crumpled PMMA-g-G sheets in the final crumpled state, which provides insight into the internal structure and mechanical state of the crumpled sheets with different grafting densities g. **Figure 5(a)** and **(b)** show the distributions of K and σ_v of the crumpled PMMA-g-G sheets with g of 0.004, 0.15, and 0.4 chains/nm^2. In this study, K and σ_v are mapped to a 2D planar model for better visualization. It can be observed that both the high K and high σ_v regions of the crumpled sheets decrease significantly as g increases from 0.004 chains/nm^2 to 0.4 chains/nm^2. Moreover, the "dense" stress network of the crumpled sheet with small grafting density become "sparse" in large grafting density cases, suggesting that the degree of mechanical heterogeneity of the crumpled sheets decreases with increasing grafting density. **Figure 5(c)** presents the distribution of K versus σ_v for crumpled PMMA-g-G sheets having various g. It is evident that the overall K and σ_v are smaller for the crumpled sheet with larger g; K and σ_v maintain a certain correlation: large K corresponds to large σ_v and small K corresponds to small σ_v.

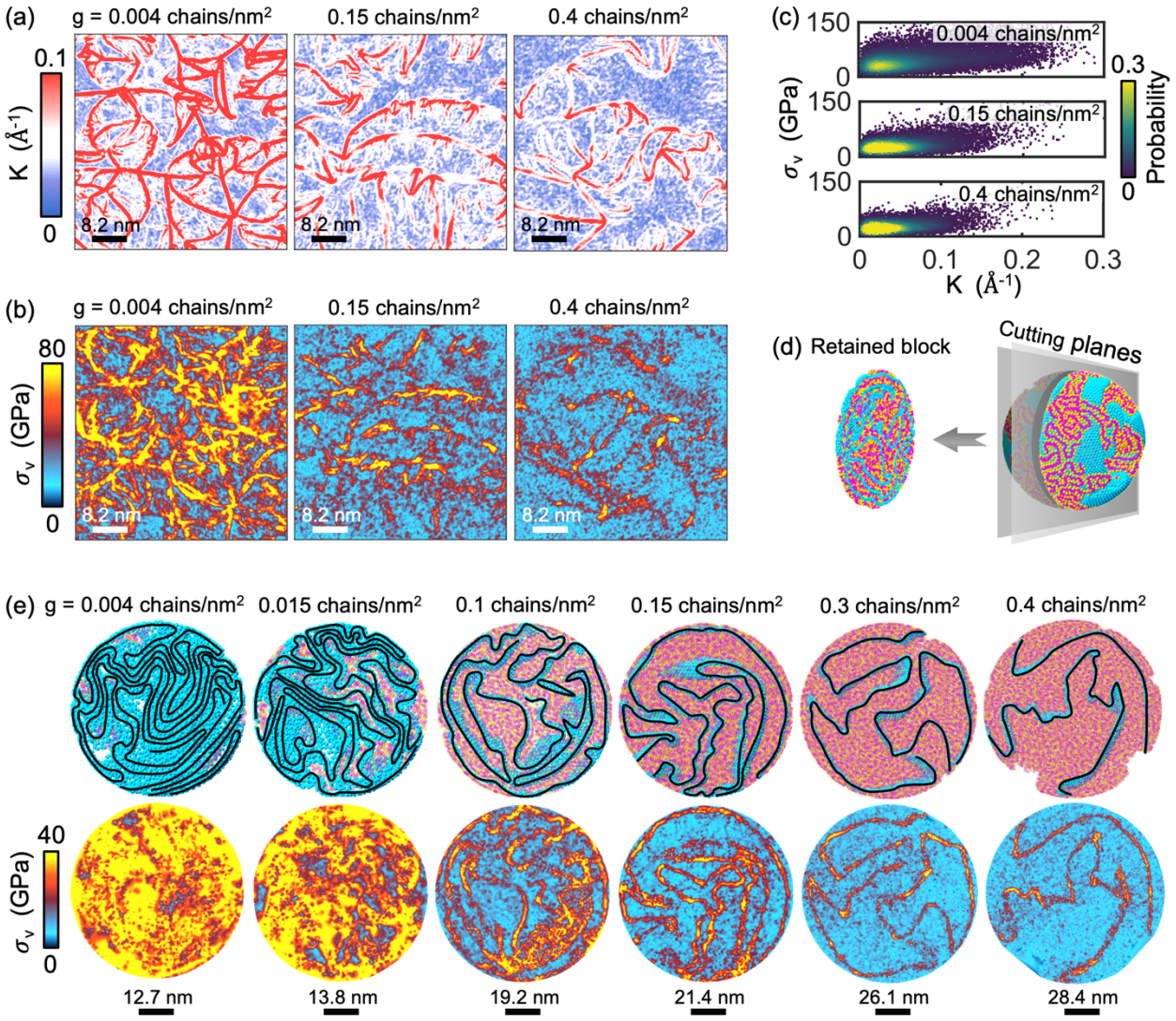

Figure 5. Mechanical state of crumpled PMMA-g-G sheets in the final crumpled state. Maps of **(a)** the local curvature K and **(b)** local von Mises stress σ_v distributions for crumpled PMMA-g-G sheets with different grafting densities g. **(c)** Distribution of K versus σ_v for crumpled sheets with different g. **(d)** Schematic for analyzing the cross-section pattern of the crumpled sheets. The retained block has a thickness of 1 nm, which is obtained by cutting planes located on both sides of the center of mass of the crumpled sphere. **(e)** The cross-section patterns and their stress σ_v distributions for crumpled sheets having various g. The cross-section of graphene is highlighted with a black curve, and the black and white lines represent the scale bar.

To gain a deeper insight into the influence of grafting density on the internal structures of the crumpled PMMA-g-G sheets, we discuss here the cross-section patterns

and stress distributions in the cross-sections of the crumpled sheets. As shown in **Figure 5(d)**, we obtain a retained block (1 nm thickness) by cutting the crumpled model with two virtual cutting planes. The cross-section pattern of the crumpled system and its stress distribution can be analysed based on the retained block. It can be found from **Figure 5(e)** that the cross section has comparatively ordered, laminated, and compacted graphene folds in the crumpled sheet with small grafting densities (*e.g.*, 0.004 and 0.015 chains/nm^2), while it shows a disordered and less folded pattern and most of the region is occupied by PMMA beads in the case of large grafting densities (e.g., 0.15, 0.3, and 0.4 chains/nm^2(. In other words, the volume of the final crumpled sheets increases as the grafting density increases (its radius is controlled by Eqn. (3)), allowing the graphene sheets to fold less. Note that the sizes of the graphene sheets considered here are fixed and neither graphene nor PMMA undergo amorphous collapse or damage (*e.g.*, bond broken) in the final crumpled state. **Figure 5(e)** further shows the local Von Mises stress σ_v distribution in the cross-section. Specifically, the high stress region decreases with increasing grafting density, implying a reduced degree of mechanical heterogeneity in the cross-section. In addition, the graphene beads have greater σ_v than PMMA, since graphene (the strongest material known) has greater bonded interactions and adhesion than PMMA. It should be noted that while numerical discrepancies may exist between our simulations and experiment due to the model and simulation setup, the mechanically heterogeneous patterns derived from the simulations are expected to exhibit a high degree of correlation with the experimental observations.

4. Conclusions

In this work, we investigated the conformation at equilibrium, crumpling behavior, and mechanical state of PMMA-g-G nanosheets based on CG-MD simulations by systematically varying the grafting density of the system at a fixed sheet width. We find that the grafting density of PMMA-g-G sheets strongly controls the conformation, crumpling process, internal crumpled structure, and mechanical state of the sheets at the molecular level. Specifically, the conformation of PMMA-g-G sheets in the initial equilibrium is divided into three different regimes based on the range of grafting densities g, corresponding to the flat ($0 \leq g \lesssim 0.05$ chains/nm^2), folded (0.05 chains/nm$^2 \lesssim g \lesssim 0.275$ chains/nm^2), and wrinkled ($g \gtrsim 0.275$ chains/nm^2) states (see **Figure 2(b)**). In the folded and wrinkled regimes, the sheet configuration is governed by the local distribution of PMMA—regions of small PMMA distribution correspond to large sheet curvature. Moreover, evaluation of the total potential energy and relative shape anisotropy reveals enhanced bending behavior and reduced self-adhering and self-folding behaviors of the sheets in the folded and wrinkled regimes during the crumpling process. Additionally, our results show that the local stress has strong correlation with the local curvature of graphene sheets in the crumpled system, and increasing the grafting density reduces the mechanical heterogeneity of the crumpled system. Finally, analysis of the cross-section patterns highlights the shift in the internal structure of the crumpled system from relatively ordered, laminated, and compacted graphene folds to disordered and less folded pattern filled with PMMA as the grafting density increases.

Herein, the understanding of PMMA-g-G sheets conformation is crucial to extend their applications such as in nanocomposites and drug delivery fields. In nanocomposites, the conformation of PMMA-g-G directly affects the mechanical strength, thermal stability, electrical

conductivity, and durability of the material.[26] In drug delivery systems, the slow-release of drugs can be achieved by controlling the conformation of polymer-grafted sheets, which is essential for achieving targeted therapies, improving therapeutic efficacy, and reducing side effects.[70] The biocompatibility and dispersibility of polymer grafted sheets in biological fluids or polymer matrices can be improved by manipulating their conformations, which ensures homogeneity and stability of the drug delivery system as well as optimizing the properties of the nanocomposites. Our study highlights the critical influence of grafting density on the structure of crumpled PMMA-g-G nanosheets, providing essential insights for the future tailored design of crumpled polymer grafted nanosheets for functional nanocomposite applications.

Conflict of Interest

The authors declare no interest conflict.

Acknowledgements

The authors acknowledge the support from the National Science Foundation (NSF) under NSF CMMI Award No. 2237063. The authors also acknowledge the support from the Department of Aerospace Engineering and College of Engineering at Iowa State University.

References

(1) Novoselov, K. S.; Geim, A. K.; Morozov, S. V.; Jiang, D.; Zhang, Y.; Dubonos, S. V.; Grigorieva, I. V.; Firsov, A. A. Electric Field in Atomically Thin Carbon Films. *Science.* **2004**, *306* (5696), 666–669. https://doi.org/10.1126/science.1102896.

(2) Sakhaee-Pour, A. Elastic Buckling of Single-Layered Graphene Sheet. *Comput. Mater. Sci.* **2009**, *45* (2), 266–270. https://doi.org/https://doi.org/10.1016/j.commatsci.2008.09.024.

(3) Pereira, V. M.; Castro Neto, A. H.; Liang, H. Y.; Mahadevan, L. Geometry, Mechanics, and Electronics of Singular Structures and Wrinkles in Graphene. *Phys. Rev. Lett.* **2010**, *105* (15), 156603. https://doi.org/10.1103/PhysRevLett.105.156603.

(4) Liu, B.; Reddy, C. D.; Jiang, J.; Baimova, J. A.; Dmitriev, S. V.; Nazarov, A. A.; Zhou, K. Morphology and In-Plane Thermal Conductivity of Hybrid Graphene Sheets. *Appl. Phys. Lett.* **2012**, *101* (21), 211909. https://doi.org/10.1063/1.4767388.

(5) Wang, J.; Ma, F.; Liang, W.; Wang, R.; Sun, M. Optical, Photonic and Optoelectronic Properties of Graphene, h-NB and Their Hybrid Materials. *Nanophotonics*. **2017**, 943–976. https://doi.org/10.1515/nanoph-2017-0015.

(6) Luan, V. H.; Tien, H. N.; Hoa, L. T.; Hien, N. T. M.; Oh, E. S.; Chung, J.; Kim, E. J.; Choi, W. M.; Kong, B. S.; Hur, S. H. Synthesis of a Highly Conductive and Large Surface Area Graphene Oxide Hydrogel and Its Use in a Supercapacitor. *J. Mater. Chem. A* **2013**, *1* (2), 208–211. https://doi.org/10.1039/c2ta00444e.

(7) Stankovich, S.; Dikin, D. A.; Dommett, G. H. B.; Kohlhaas, K. M.; Zimney, E. J.; Stach, E. A.; Piner, R. D.; Nguyen, S. B. T.; Ruoff, R. S. Graphene-Based Composite Materials. *Nature* **2006**, *442* (7100), 282–286. https://doi.org/10.1038/nature04969.

(8) Grantab, R.; Shenoy, V. B.; Ruoff, R. S.; Lee, S.; Zande, A. van der; Petrone, N.; Hammerberg, A. G.; Lee, C.; Crawford, B.; Oliver, W.; Kysar, J. W.; Hone, J. Anomalous Strength Characteristics of Tilt Grain Boundaries in Graphene. *Science.* **2010**, *330* (6006), 946–948. https://doi.org/10.1126/science.1196893.

(9) Kempaiah, R.; Chung, A.; Maheshwari, V. Graphene as Cellular Interface: Electromechanical Coupling with Cells. *ACS Nano*. **2011**, 5, 6025–6031. https://doi.org/10.1021/nn201791k.

(10) Yang, X.; Cheng, C.; Wang, Y.; Qiu, L.; Li, D. Liquid-Mediated Dense Integration of Graphene Materials for Compact Capacitive Energy Storage. *Science.* **2013**, *341* (6145), 534–537. https://doi.org/10.1126/science.1239089.

(11) Dean, C. R.; Young, A. F.; Meric, I.; Lee, C.; Wang, L.; Sorgenfrei, S.; Watanabe, K.; Taniguchi, T.; Kim, P.; Shepard, K. L.; Hone, J. Boron Nitride Substrates for High-Quality Graphene Electronics. *Nat. Nanotechnol.* **2010**, *5* (10), 722–726. https://doi.org/10.1038/nnano.2010.172.

(12) Potts, J. R.; Dreyer, D. R.; Bielawski, C. W.; Ruoff, R. S. Graphene-Based Polymer Nanocomposites. *Polymer*. 2011, pp 5–25. https://doi.org/10.1016/j.polymer.2010.11.042.

(13) Park, S.; He, S.; Wang, J.; Stein, A.; Macosko, C. W. Graphene-Polyethylene Nanocomposites: Effect of Graphene Functionalization. *Polymer (Guildf).* **2016**, *104*, 1–9. https://doi.org/10.1016/j.polymer.2016.09.058.

(14) Chee, W. K.; Lim, H. N.; Huang, N. M.; Harrison, I. Nanocomposites of Graphene/Polymers: A Review. *RSC Adv.* **2015**, *5* (83), 68014–68051. https://doi.org/10.1039/c5ra07989f.

(15) Xu, Z.; Gao, C. In Situ Polymerization Approach to Graphene-Reinforced Nylon-6

Composites. *Macromolecules* **2010**, *43* (16), 6716–6723. https://doi.org/10.1021/ma1009337.

(16) Subbiah, T.; Bhat, G. S.; Tock, R. W.; Parameswaran, S.; Ramkumar, S. S. Electrospinning of Nanofibers. *J. Appl. Polym. Sci.* **2005**, *96* (2), 557–569. https://doi.org/10.1002/app.21481.

(17) Lee, S. J.; Yoon, S. J.; Jeon, I.-Y. Graphene/Polymer Nanocomposites: Preparation, Mechanical Properties, and Application. *Polymers (Basel).* **2022**, *14* (21), 4733. https://doi.org/10.3390/polym14214733.

(18) Lotya, M.; Hernandez, Y.; King, P. J.; Smith, R. J.; Nicolosi, V.; Karlsson, L. S.; Blighe, F. M.; De, S.; Zhiming, W.; McGovern, I. T.; Duesberg, G. S.; Coleman, J. N. Liquid Phase Production of Graphene by Exfoliation of Graphite in Surfactant/Water Solutions. *J. Am. Chem. Soc.* **2009**, *131* (10), 3611–3620. https://doi.org/10.1021/ja807449u.

(19) Konatham, D.; Striolo, A. Molecular Design of Stable Graphene Nanosheets Dispersions. *Nano Lett.* **2008**, *8* (12), 4630–4641. https://doi.org/10.1021/nl802262p.

(20) Eskandari, P.; Abousalman-Rezvani, Z.; Roghani-Mamaqani, H.; Salami-Kalajahi, M.; Mardani, H. Polymer Grafting on Graphene Layers by Controlled Radical Polymerization. *Advances in Colloid and Interface Science*. 2019. https://doi.org/10.1016/j.cis.2019.102021.

(21) Gao, L.; Ni, G. X.; Liu, Y.; Liu, B.; Castro Neto, A. H.; Loh, K. P. Face-to-Face Transfer of Wafer-Scale Graphene Films. *Nature* **2014**, *505* (7482), 190–194. https://doi.org/10.1038/nature12763.

(22) Zang, J.; Ryu, S.; Pugno, N.; Wang, Q.; Tu, Q.; Buehler, M. J.; Zhao, X. Multifunctionality and Control of the Crumpling and Unfolding of Large-Area Graphene.

Nat. Mater. **2013**, *12* (4), 321–325. https://doi.org/10.1038/nmat3542.

(23) Shenoy, V. B.; Reddy, C. D.; Ramasubramaniam, A.; Zhang, Y. W. Edge-Stress-Induced Warping of Graphene Sheets and Nanoribbons. *Phys. Rev. Lett.* **2008**, *101* (24). https://doi.org/10.1103/PhysRevLett.101.245501.

(24) Seung, H. S.; Nelson, D. R. Defects in Flexible Membranes with Crystalline Order. *Phys. Rev. A* **1988**, *38* (2), 1005–1018. https://doi.org/10.1103/PhysRevA.38.1005.

(25) Dehnert, M.; Spitzner, E. C.; Beckert, F.; Friedrich, C.; Magerle, R. Subsurface Imaging of Functionalized and Polymer-Grafted Graphene Oxide. *Macromolecules* **2016**, *49* (19), 7415–7425. https://doi.org/10.1021/acs.macromol.6b01519.

(26) Wang, Y.; Meng, Z. Mechanical and Viscoelastic Properties of Wrinkled Graphene Reinforced Polymer Nanocomposites – Effect of Interlayer Sliding within Graphene Sheets. *Carbon N. Y.* **2021**, *177*, 128–137. https://doi.org/10.1016/j.carbon.2021.02.071.

(27) Ramanathan, T.; Abdala, A. A.; Stankovich, S.; Dikin, D. A.; Herrera-Alonso, M.; Piner, R. D.; Adamson, D. H.; Schniepp, H. C.; Chen, X.; Ruoff, R. S.; Nguyen, S. T.; Aksay, I. A.; Prud'Homme, R. K.; Brinson, L. C. Functionalized Graphene Sheets for Polymer Nanocomposites. *Nat. Nanotechnol.* **2008**, *3* (6), 327–331. https://doi.org/10.1038/nnano.2008.96.

(28) Zhang, B.; Chen, Y. U.; Zhuang, X.; Liu, G.; Yu, B.; Kang, E. T.; Zhu, J.; Li, Y. Poly(N-Vinylcarbazole) Chemically Modified Graphene Oxide. *J. Polym. Sci. Part A Polym. Chem.* **2010**, *48* (12), 2642–2649. https://doi.org/10.1002/pola.24047.

(29) Fang, M.; Wang, K.; Lu, H.; Yang, Y.; Nutt, S. Single-Layer Graphene Nanosheets with Controlled Grafting of Polymer Chains. *J. Mater. Chem.* **2010**, *20* (10), 1982–1992. https://doi.org/10.1039/b919078c.

(30) Ye, Y. S.; Chen, Y. N.; Wang, J. S.; Rick, J.; Huang, Y. J.; Chang, F. C.; Hwang, B. J. Versatile Grafting Approaches to Functionalizing Individually Dispersed Graphene Nanosheets Using RAFT Polymerization and Click Chemistry. *Chem. Mater.* **2012**, *24* (15), 2987–2997. https://doi.org/10.1021/cm301345r.

(31) Zhang, J.; Zuo, M.; Lv, X.; Zhang, H.; Zheng, Q. Effect of Grafted Graphene Nanosheets on Morphology Evolution and Conductive Behavior of Poly(Methyl Methacrylate)/Poly(Styrene-: Co -Acrylonitrile) Blends during Isothermal Annealing. *RSC Adv.* **2018**, *8* (26), 14579–14588. https://doi.org/10.1039/c8ra00439k.

(32) Sekhavat Pour, Z.; Ghaemy, M. Polymer Grafted Graphene Oxide: For Improved Dispersion in Epoxy Resin and Enhancement of Mechanical Properties of Nanocomposite. *Compos. Sci. Technol.* **2016**, *136*, 145–157. https://doi.org/10.1016/j.compscitech.2016.10.014.

(33) Wang, X.; Xing, W.; Zhang, P.; Song, L.; Yang, H.; Hu, Y. Covalent Functionalization of Graphene with Organosilane and Its Use as a Reinforcement in Epoxy Composites. *Compos. Sci. Technol.* **2012**, *72* (6), 737–743. https://doi.org/10.1016/j.compscitech.2012.01.027.

(34) Li, W.; Xu, Z.; Chen, L.; Shan, M.; Tian, X.; Yang, C.; Lv, H.; Qian, X. A Facile Method to Produce Graphene Oxide-g-Poly(L-Lactic Acid) as an Promising Reinforcement for PLLA Nanocomposites. *Chem. Eng. J.* **2014**, *237*, 291–299. https://doi.org/10.1016/j.cej.2013.10.034.

(35) Xia, W.; Pestana, L. R. *Fundamentals of Multiscale Modeling of Structural Materials*, 1st Editio.; Elsevier, 2022.

(36) Bae, S.; Galant, O.; Diesendruck, C. E.; Silberstein, M. N. The Effect of Intrachain Cross-

Linking on the Thermomechanical Behavior of Bulk Polymers Assembled Solely from Single Chain Polymer Nanoparticles. *Macromolecules* **2018**, *51* (18), 7160–7168. https://doi.org/10.1021/acs.macromol.8b01027.

(37) Liu, M.; Li, S.; Fang, Y.; Chen, Z.; Alyas, M.; Liu, J.; Zeng, X.; Zhang, L. Mechanical and Self-Healing Behavior of Matrix-Free Polymer Nanocomposites Constructed via Grafted Graphene Nanosheets. *Langmuir* **2020**, *36* (26), 7427–7438. https://doi.org/10.1021/acs.langmuir.0c00971.

(38) Yousefi, N.; Lin, X.; Zheng, Q.; Shen, X.; Pothnis, J. R.; Jia, J.; Zussman, E.; Kim, J. K. Simultaneous in Situ Reduction, Self-Alignment and Covalent Bonding in Graphene Oxide/Epoxy Composites. *Carbon N. Y.* **2013**, *59*, 406–417. https://doi.org/10.1016/j.carbon.2013.03.034.

(39) Yousefi, N.; Sun, X.; Lin, X.; Shen, X.; Jia, J.; Zhang, B.; Tang, B.; Chan, M.; Kim, J. K. Highly Aligned Graphene/Polymer Nanocomposites with Excellent Dielectric Properties for High-Performance Electromagnetic Interference Shielding. *Adv. Mater.* **2014**, *26* (31), 5480–5487. https://doi.org/10.1002/adma.201305293.

(40) Kim, J. Y.; Lee, J. H.; Grossman, J. C. Thermal Transport in Functionalized Graphene. *ACS Nano* **2012**, *6* (10), 9050–9057. https://doi.org/10.1021/nn3031595.

(41) Shen, X.; Wang, Z.; Wu, Y.; Liu, X.; Kim, J. K. Effect of Functionalization on Thermal Conductivities of Graphene/Epoxy Composites. *Carbon N. Y.* **2016**, *108*, 412–422. https://doi.org/10.1016/j.carbon.2016.07.042.

(42) Zhang, X.; Wu, L.; Wang, J. Distinct Mechanical Properties of Polymer/Polymer-Grafting-Graphene Nanocomposites. *Macromol. Chem. Phys.* **2018**, *219* (14), 1800161. https://doi.org/https://doi.org/10.1002/macp.201800161.

(43) Croll, A. B.; Liao, Y.; Li, Z.; Jayawardana, W. M. A.; Elder, T.; Xia, W. Sticky Crumpled Matter. *Matter* **2022**, *5* (6), 1792–1805. https://doi.org/10.1016/j.matt.2022.04.029.

(44) Jayawardana, W. M. A.; Liao, Y.; Li, Z.; Xia, W.; Croll, A. B. Crumpled Kirigami. *Soft Matter* **2023**, *19* (6), 1081–1091. https://doi.org/10.1039/d2sm01584f.

(45) Baimova, J. A.; Korznikova, E. A.; Dmitriev, S. V.; Liu, B.; Zhou, K. Review on Crumpled Graphene: Unique Mechanical Properties. *Rev. Adv. Mater. Sci.* **2014**, *39* (1).

(46) El Rouby, W. M. A. Crumpled Graphene: Preparation and Applications. *RSC Adv.* **2015**, *5* (82), 66767–66796. https://doi.org/10.1039/c5ra10289h.

(47) Wang, C.; Liu, Y.; Li, L.; Tan, H. Anisotropic Thermal Conductivity of Graphene Wrinkles. *Nanoscale* **2014**, *6* (11), 5703–5707. https://doi.org/10.1039/c4nr00423j.

(48) Huang, H.; Rao, P.; Choi, W. M. Carbon-Coated Silicon/Crumpled Graphene Composite as Anode Material for Lithium-Ion Batteries. *Curr. Appl. Phys.* **2019**, *19* (12), 1349–1354. https://doi.org/10.1016/j.cap.2019.08.024.

(49) Hao, W.; Chiou, K.; Qiao, Y.; Liu, Y.; Song, C.; Deng, T.; Huang, J. Crumpled Graphene Ball-Based Broadband Solar Absorbers. *Nanoscale* **2018**, *10* (14), 6306–6312. https://doi.org/10.1039/c7nr09556b.

(50) Dou, X.; Koltonow, A. R.; He, X.; Jang, H. D.; Wang, Q.; Chung, Y. W.; Huang, J. Self-Dispersed Crumpled Graphene Balls in Oil for Friction and Wear Reduction. *Proc. Natl. Acad. Sci. U. S. A.* **2016**, *113* (6), 1528–1533. https://doi.org/10.1073/pnas.1520994113.

(51) Wang, Y.; Yang, R.; Shi, Z.; Zhang, L.; Shi, D.; Wang, E.; Zhang, G. Super-Elastic Graphene Ripples for Flexible Strain Sensors. *ACS Nano* **2011**, *5* (5), 3645–3650. https://doi.org/10.1021/nn103523t.

(52) Hsu, D. D.; Xia, W.; Arturo, S. G.; Keten, S. Systematic Method for Thermomechanically

Consistent Coarse-Graining: A Universal Model for Methacrylate-Based Polymers. *J. Chem. Theory Comput.* **2014**, *10* (6), 2514–2527. https://doi.org/10.1021/ct500080h.

(53) Ruiz, L.; Xia, W.; Meng, Z.; Keten, S. A Coarse-Grained Model for the Mechanical Behavior of Multi-Layer Graphene. *Carbon N. Y.* **2015**, *82* (C), 103–115. https://doi.org/10.1016/j.carbon.2014.10.040.

(54) Ma, X.; Zachariah, M. R.; Zangmeister, C. D. Crumpled Nanopaper from Graphene Oxide. *Nano Lett.* **2012**, *12* (1), 486–489. https://doi.org/10.1021/nl203964z.

(55) Xia, W.; Vargas-Lara, F.; Keten, S.; Douglas, J. F. Structure and Dynamics of a Graphene Melt. *ACS Nano* **2018**, *12* (6), 5427–5435. https://doi.org/10.1021/acsnano.8b00524.

(56) Yang, Z.; Chiang, C. C.; Meng, Z. Investigation of Dynamic Impact Responses of Layered Polymer-Graphene Nanocomposite Films Using Coarse-Grained Molecular Dynamics Simulations. *Carbon N. Y.* **2023**, *203*, 202–210. https://doi.org/10.1016/j.carbon.2022.11.015.

(57) Chen, X.; Zheng, M.; Park, C.; Ke, C. Direct Measurements of the Mechanical Strength of Carbon Nanotube-Poly(Methyl Methacrylate) Interfaces. *Small* **2013**, *9* (19), 3345–3351. https://doi.org/10.1002/smll.201202771.

(58) Liao, Y.; Li, Z.; Ghazanfari, S.; Fatima; Croll, A. B.; Xia, W. Understanding the Role of Self-Adhesion in Crumpling Behaviors of Sheet Macromolecules. *Langmuir* **2021**, *37* (28), 8627–8637. https://doi.org/10.1021/acs.langmuir.1c01545.

(59) Liao, Y.; Li, Z.; Fatima; Xia, W. Size-Dependent Structural Behaviors of Crumpled Graphene Sheets. *Carbon N. Y.* **2021**, *174*, 148–157. https://doi.org/10.1016/j.carbon.2020.12.006.

(60) Liao, Y.; Li, Z.; Nie, W.; Xia, W. Effect of Reconstructed Vacancy Defects on the

Crumpling Behavior of Graphene Sheets. *Forces Mech.* **2022**, *6*, 100057. https://doi.org/10.1016/j.finmec.2021.100057.

(61) Liao, Y.; Li, Z.; Chen, L.; Croll, A. B.; Xia, W. Crumpling Defective Graphene Sheets. *Nano Lett.* **2023**, *23* (8), 3637–3644. https://doi.org/10.1021/acs.nanolett.2c04771.

(62) Plimpton, S. Fast Parallel Algorithms for Short-Range Molecular Dynamics. *J. Comput. Phys.* **1995**, *117* (1), 1–19. https://doi.org/10.1006/jcph.1995.1039.

(63) Humphrey, W.; Dalke, A.; Schulten, K. VMD: Visual Molecular Dynamics. *J. Mol. Graph.* **1996**, *14* (1), 33–38. https://doi.org/10.1016/0263-7855(96)00018-5.

(64) Arkin, H.; Janke, W. Gyration Tensor Based Analysis of the Shapes of Polymer Chains in an Attractive Spherical Cage. *J. Chem. Phys.* **2013**, *138* (5). https://doi.org/10.1063/1.4788616.

(65) Warner, J. H.; Rümmeli, M. H.; Ge, L.; Gemming, T.; Montanari, B.; Harrison, N. M.; Büchner, B.; Briggs, G. A. D. Structural Transformations in Graphene Studied with High Spatial and Temporal Resolution. *Nat. Nanotechnol.* **2009**, *4* (8), 500–504. https://doi.org/10.1038/nnano.2009.194.

(66) Laradji, M. A Monte Carlo Study of Fluctuating Polymer-Grafted Membranes. *J. Chem. Phys.* **2004**, *121* (3). https://doi.org/10.1063/1.1763839.

(67) Metzler, R.; Hanke, A.; Dommersnes, P. G.; Kantor, Y.; Kardar, M. Tightness of Slip-Linked Polymer Chains. *Phys. Rev. E - Stat. Physics, Plasmas, Fluids, Relat. Interdiscip. Top.* **2002**, *65* (6). https://doi.org/10.1103/PhysRevE.65.061103.

(68) Cranford, S. W.; Buehler, M. J. Packing Efficiency and Accessible Surface Area of Crumpled Graphene. *Phys. Rev. B - Condens. Matter Mater. Phys.* **2011**, *84* (20), 205451. https://doi.org/10.1103/PhysRevB.84.205451.

(69) Becton, M.; Zhang, L.; Wang, X. Mechanics of Graphyne Crumpling. *Phys. Chem. Chem. Phys.* **2014**, *16* (34), 18233–18240. https://doi.org/10.1039/c4cp02400a.

(70) Najafi rad, Z.; Farzad, F.; Razavi, L. Surface Functionalization of Graphene Nanosheet with Poly (l-Histidine) and Its Application in Drug Delivery: Covalent vs Non-Covalent Approaches. *Sci. Rep.* **2022**, *12* (1), 19046. https://doi.org/10.1038/s41598-022-21619-0.

Table of Contents (TOC) graphic